



# Nitrogen-doped carbon frameworks decorated with palladium nanoparticles for simultaneous electrochemical voltammetric determination of uric acid and dopamine in the presence of ascorbic acid

Yao Yao<sup>1</sup> · Ji Zhong<sup>1</sup> · Zhiwei Lu<sup>1</sup> · Xin Liu<sup>1</sup> · Yanying Wang<sup>1</sup> · Tao Liu<sup>2</sup> · Ping Zou<sup>1</sup> · Xianxiang Dai<sup>1</sup> · Xianxiang Wang<sup>1</sup> · Fang Ding<sup>3</sup> · Cailong Zhou<sup>4</sup> · Qingbiao Zhao<sup>5</sup> · Hanbing Rao<sup>1</sup>

Received: 26 May 2019 / Accepted: 11 October 2019 / Published online: 16 November 2019  
© Springer-Verlag GmbH Austria, part of Springer Nature 2019

## Abstract

A glassy carbon electrode (GCE) was modified with nitrogen-enriched carbon frameworks decorated with palladium nanoparticles (Pd@NCF/GCEs). The modified GCE is shown to be a viable tool for determination of uric acid (UA) and dopamine (DA) in the presence of ascorbic acid (AA). The Pd@NCF was fabricated through one-step pyrolysis and characterized by X-ray photoelectron spectroscopy, X-ray diffraction, scanning electron microscopy and nitrogen-adsorption/desorption analysis. The Pd@NCF/GCE was characterized by differential pulse voltammetry (DPV). Both UA and DA have pronounced oxidation peaks (at 360 mV for UA and 180 mV for DA, all vs. Ag/AgCl) in the presence of AA. Response is linear in the 0.5–100  $\mu\text{M}$  UA concentration range and in the 0.5–230  $\mu\text{M}$  DA concentration range. The detection limits are 76 and 107 nM, respectively (at  $S/N = 3$ ). This electrode is stable, reproducible and highly selective. It was used for UA and DA determination in spiked serum samples.

**Keywords** Electrochemical sensor · Simultaneous determination · Non-enzymatic · Amperometric response · Modified electrode · Biological small molecule

## Introduction

Uric acid (UA), dopamine (DA) and ascorbic acid (AA) are important in the process of human metabolism [1]. Simultaneous or individually determination of DA, UA and AA has become important [2, 3]. Various techniques have

been used to detect these compounds, such as spectrophotometry [4], fluorescence spectroscopy [5], surface plasmon resonance [6], chemiluminescence [7] and electrochemical method [8, 9]. Electrochemical methods have the advantages of being convenient, rapid and sensitive. Considering that DA, UA, and AA have high electrochemical activity,

**Electronic supplementary material** The online version of this article (<https://doi.org/10.1007/s00604-019-3907-6>) contains supplementary material, which is available to authorized users.

✉ Qingbiao Zhao  
qbzhao@ee.ecnu.edu.cn

✉ Hanbing Rao  
rhb@sicau.edu.cn

<sup>1</sup> College of Science, Sichuan Agricultural University, Xin Kang Road, Yucheng District, Ya'an 625014, People's Republic of China

<sup>2</sup> College of Information Engineering, Sichuan Agricultural University, Xin Kang Road, Yucheng District, Ya'an 625014, People's Republic of China

<sup>3</sup> Nanshan District Key Lab for Biopolymers and Safety Evaluation, Shenzhen Key Laboratory of Polymer Science and Technology, Guangdong Research Center for Interfacial Engineering of Functional Materials, College of Materials Science and Engineering, Shenzhen University, Shenzhen 518060, People's Republic of China

<sup>4</sup> School of Chemistry and Chemical Engineering, Chongqing University, Chongqing 400044, People's Republic of China

<sup>5</sup> Key Laboratory of Polar Materials and Devices (MOE), Department of Optoelectronics, East China Normal University, Shanghai 200241, People's Republic of China

electrochemical techniques can be used to simultaneously determine these biomolecules. However, the main obstacle is that AA, UA, and DA electrochemical oxidation potentials are similar, resulting in overlapping voltammetry responses with poor selectivity and inaccurate quantitative analysis, making it difficult to simultaneously determine them [10, 11]. Besides, AA concentration in body fluids is 1000 times that of DA. Therefore, selective analysis of UA and DA containing relatively high concentration of AA is important for diagnosis and pathological study.

It is well known that selective detection of these electroactive biomolecules has been realized with nanomaterials. Li et al. [10] reported the detection of UA and DA in the presence of high concentration of AA (1.0 mM) by silver nanocube functionalized dopamine nanospheres and carboxyl-functionalized graphene co-modified gold electrode (AgNC@PDA-NS/CGF/GCE). Sroysee et al. [11] reported that carbon nanotubes-paste electrode was modified with poly(m-ferrocenylaniline) and covered with Nafion film for detection of UA and DA coexisting with AA. In these studies, Nafion film modified electrodes were often used. However, the negatively charged polymer film modified electrode has limitations, such as poor conductivity and poor stability, etc. [12]. Thus, it is important to enhance the electroanalytical performance of electrochemical sensing systems for UA and DA.

Precious metal nanoparticles (NPs), such as Pt, Ag, Au, and Pd have been widely used in electrochemical applications, such as electrocatalysis and electroanalysis of small biomolecules, due to their unique physicochemical properties [13]. Among them, Pd NPs have become an important research topic due to its relatively lower cost and larger abundance compared with Au NPs and Pt NPs [14, 15]. However, Pd NPs easily aggregate due to the high surface free energy [16], resulting in decreased catalytic activity. Carbon-based nanomaterials have been widely used as supports due to their high conductivity, excellent stability, as well as large surface area [17]. Therefore, the combination of Pd NPs and carbon-based nanomaterials provide more active sites for the adsorption of biomolecules, leading to higher electrocatalytic performance.

Herein, a facile method for preparing 3D nitrogen-doped carbon frameworks loaded with Pd NPs (Pd@NCFs) nanocomposites is reported. The 3D Pd@NCFs nanocomposites were conveniently prepared via one-step pyrolysis of PVP and palladium nitrate. Pd@NCFs nanocomposites possess nanoporous carbon foam-like structure, large surface area as well as good electrical conductivity. As a result, Pd@NCFs modified GCE (Pd@NCFs/GCE) shows good electrocatalytic activity toward UA and DA. Finally, the Pd@NCFs/GCE

was utilized for simultaneous analysis of UA and DA in the presence of AA.

## Experimental

### Materials and solutions

Polyvinylpyrrolidone (PVP, K30), palladium nitrate dihydrate ( $\text{Pd}(\text{NO}_3)_2 \cdot 2\text{H}_2\text{O}$ ), N,N-dimethylformamide (DMF), AA, UA, and DA were obtained from Aladdin Biochemical Technology Co., Ltd. (Shanghai, China, <http://www.aladdin-e.com>). Ultrapure water ( $18.2 \text{ M}\Omega \cdot \text{cm}$ ) was used to prepare DA and UA solutions. The supporting electrolyte solution was phosphate buffer (PB, pH 7.0), which was composed of 0.1 M  $\text{KH}_2\text{PO}_4$ - $\text{Na}_2\text{HPO}_4$ . All reagents were of analytical grade.

### Preparation of the Pd@NCFs nanocomposite

3D Pd@NCFs nanocomposite was prepared by a convenient pyrolysis strategy. Firstly, 0.5 g PVP was dissolved into 20 mL ultrapure water, and then 150 mg  $\text{Pd}(\text{NO}_3)_2 \cdot 2\text{H}_2\text{O}$  was added. The mixtures were stirred for 1.5 h at room temperature, then kept at 120 °C overnight, allowing the mixture to be dried. Finally, the Pd@NCFs composites were obtained by pyrolysis of the precursor at 700 °C for 2 h under  $\text{N}_2$  atmosphere.

### Fabrication of 3D Pd@NCFs composites modified GCEs

Pd@NCFs (7.5 mg) were ultrasonically dispersed into 3.0 mL DMF, and a homogeneous ink suspension was obtained. Then, 0.5  $\mu\text{L}$  suspensions were drop-casted on clean GCEs and dried. The Pd@NCFs modified GCEs was defined as Pd@NCFs/GCEs and stored in an ambient environment at room temperature.

### Material characterizations and electrochemical measurement

These parts are detailed in Electronic Supplementary Materials (ESM).

### Real sample

Human serum samples were received from the Sichuan Agricultural University Hospital and diluted 10-fold with 0.1 M PB (pH 7.0). Generally, 5.0 mL of human blood serum sample was mixed with 5.0 mL of 0.1 M PB (pH 7.0) and then analyzed by the optimized DPV method. All studies were executed complying with relevant laws and guidelines.

## Results and discussion

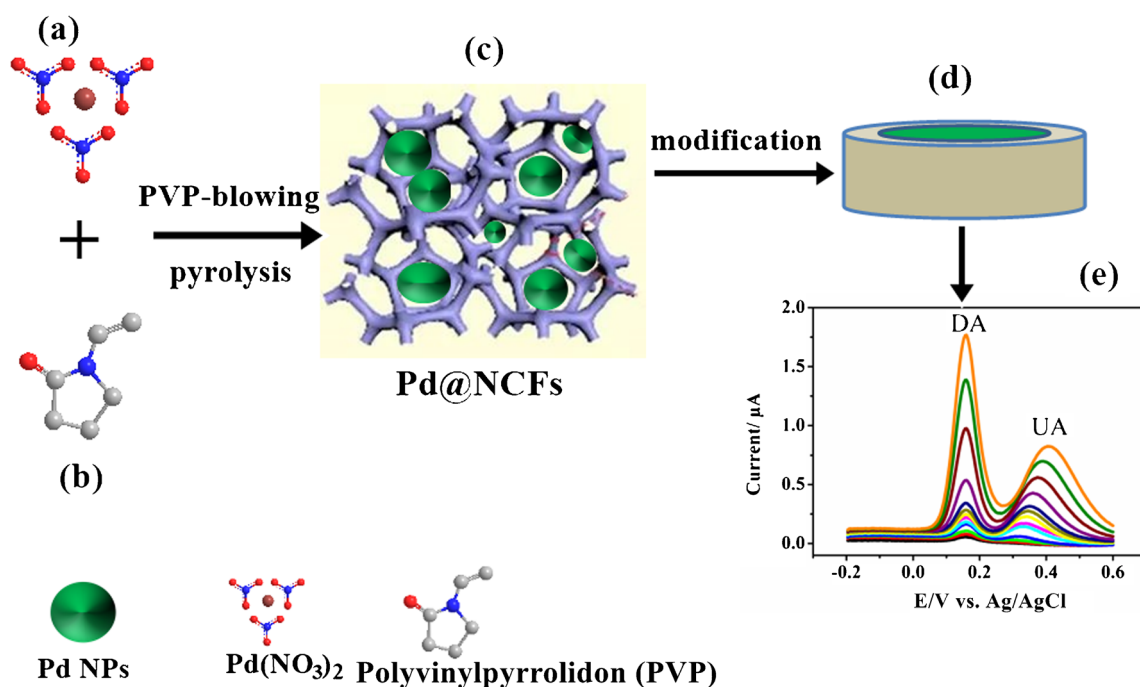
### Choice of materials

It is well known that electrode sensing materials are very important to sensitivity and selectivity of the sensor. Among the electrode modification materials, nitrogen-doped porous carbon (NPC) is a class of widely used due to its porous structure, large specific surface area, low cost and high stability. However, in previous reports, NPC materials prepared mainly include carbon post-treatment and in-situ pyrolysis of nitrogen-containing precursors, which are complicated to fabricate. In contrast, the synthesis conditions in our work are simple and facile, which via one-step pyrolysis based on polyvinylpyrrolidone-blowing (PVP-blowing) method. Nanoscale metal nanoparticle decorated NPC is an effective way to improve the sensing performance. The 3D Pd@NCFs nanocomposite as a novel and affordable modifier with unique network structure show a better separation peak and clearer oxidation peak for DA and UA in the presence of AA due to its decrease the electrode overpotential and resolve the overlapping peak potentials. This may be due to the unique catalytic properties of 3D Pd@NCFs nanocomposite. Therefore, Pd@NCFs nanocomposite modified GCE was used to simultaneously determination of DA and UA in the presence of AA. In addition, compared with Au, Pt, and other noble metals, Pd is more cost-efficient. Nanomaterials decrease the electrode overpotential and resolve the overlapping peak potentials.

### Characterizations of the 3D Pd@NCFs-800 composites

The synthetic strategy of 3D Pd@NCFs composites and electrochemical determination are illustrated in Scheme 1. The formation of Pd@NCFs can be described by a metal salt-assisted chemical blowing strategy and subsequent carbonization of PVP at high temperature [18]. Nitrogen-enriched PVP acted as a nitrogen source and carbon source, as well as the bubbling agent. Above the glass transition temperature, a large amount of gas was released by thermal-induced decomposition of palladium acetate, then molten viscous fluid of PVP was gradually inflated by the released gas, forming a bubble-like structure [19]. As the gas release and the bubbles continuously expand, the bubble walls gradually become thinned. The walls of PVP finally converted into nitrogen-doped nanoporous carbon framework at high temperature. Pd NPs were simultaneously formed through in-situ carbothermal reduction of palladium acetate at high temperature, and uniformly decorated onto the carbon matrix. This method realizes one-step in-situ fabrication of 3D Pd@NCFs composites.

The morphology of the 3D Pd@NCFs composites was characterized using SEM. As demonstrated in the low magnification SEM image (Fig. 1a, c), a typical 3D carbon framework composes of many concave porous structures, and the surface of 3D CNFs is covered by Pd nanoparticles with a high coverage ratio. Figure 1b shows the top-view high-magnification image of Pd@NCFs composite, in which there is a stacked-bowl carbon structure. The bottom of the carbon bowl is evenly decorated with Pd nanoparticles, indicating that NCFs is a good support material for Pd NPs. Besides, no obvious aggregation of Pd NPs



**Scheme 1** Schematic illustration of the preparation process of Pd@NCFs/GCE and the simultaneous electrochemical determination of UA and DA

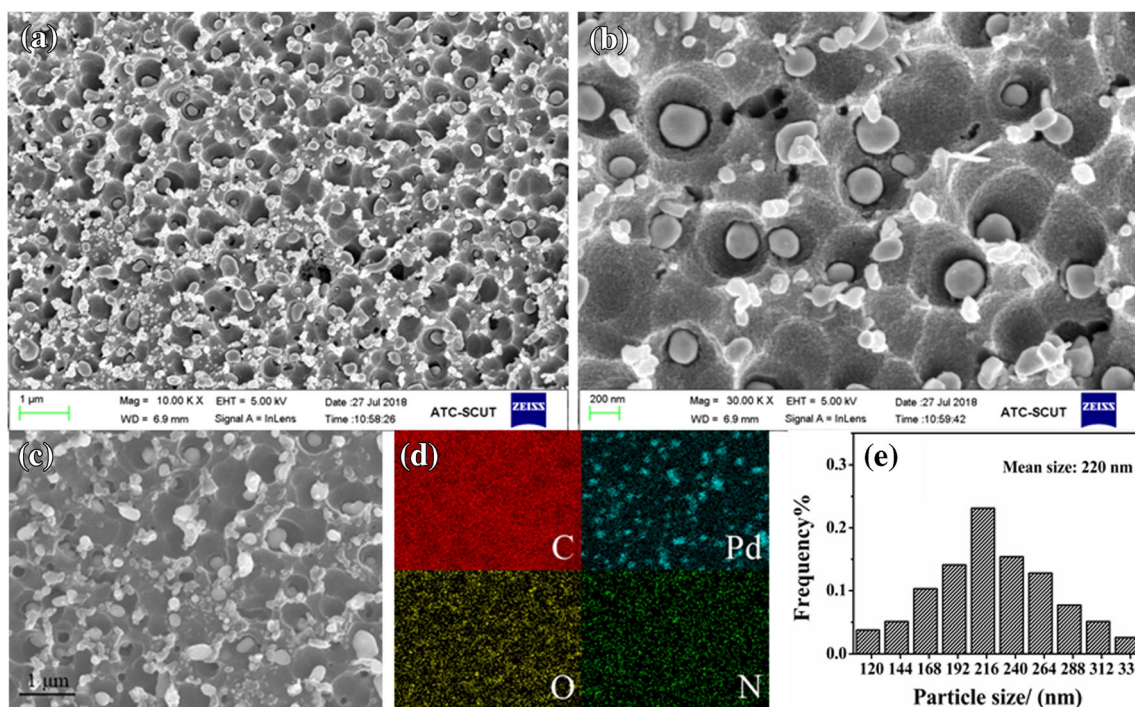


**Fig. 1** SEM images of Low (a) and high (b) magnifications of 3D Pd@NCFs nanocomposites; c SEM image of 3D Pd@NCFs and d corresponding elemental mapping of C, Pd, O, and N elements; e size distribution of Pd NPs in the 3D Pd@NCFs nanocomposites

was observed. The average size of Pd NPs is approximately 220 nm (Fig. 1e). The porous structure and uniformly dispersed Pd NPs contribute to the large surface area, accelerating the mass transfer in electrochemical applications. In addition, as shown in the corresponding elemental mapping (Fig. 1d) and the EDS pattern (Fig. S1), the 3D Pd@NCFs composites mainly consisted of C, Pd, O, and N elements, and the content of Pd atom is approximately 1.1%.

Figure S2A displays the XRD patterns of NCFs (black) and 3D Pd@NCFs composites (red), respectively. A pronounced peak located at around  $26.4^\circ$ , and a weak peak at around  $42.8^\circ$  correspond to the (002) and (101) crystal planes of graphite (Graphite 2H, JCPDS 46-1487) [17], respectively. This result indicates that graphitization occurs. Upon incorporation of Pd NPs onto NCFs substrate, five additional diffraction peaks at around  $86.6^\circ$ ,  $82.1^\circ$ ,  $68.1^\circ$ ,  $46.7^\circ$ , and  $40.1^\circ$  were observed, corresponding to the (222), (311), (220), (200) and (111) planes of Pd (JCPDS 46-1043), respectively. This result indicated that Pd(OAc)<sub>2</sub> was reduced by carbon and Pd NPs formed and its mean crystallite size was calculated as  $\sim 186$  nm with Scherrer's formula.

Raman spectroscopy provides information for distinguishing ordered and disordered carbon materials defect structures. From Fig. S2B, three sharp peaks were observed. D band is ascribed to vibration modes of defect or disordered graphite structure at  $1346\text{ cm}^{-1}$ , whereas G band corresponds to  $E_{2g}$  mode of graphitic carbons atom at  $1586\text{ cm}^{-1}$ , while the 2D band is induced by second-order zone-boundary phonons

at  $2705\text{ cm}^{-1}$  [20]. According to previous studies, the intensity ratios between G and D band ( $I_D/I_G$ ) can be applied to quantify defect in graphene material, whereas the number of stacked graphene layers can be quantified using the 2D/G intensity ratio ( $I_{2D}/I_G$ ) [21]. The  $I_D/I_G$  ratio is 1.02, suggesting that Pd@NCFs materials are a highly graphitized product. Besides, the  $I_{2D}/I_G$  ratio is 0.12, which is far less than 1, clearly indicating that Pd@NCFs was multilayer graphene foam-like structure, consistent with SEM results.

The pore structure and surface area of Pd@NCFs were studied by N<sub>2</sub> adsorption/desorption isotherms. As shown in Fig. S2C, as the relative pressure ( $P/P_0$ ) is greater than 0.45, there is a clear hysteresis loop, indicated that micropore and mesopores coexist in 3D Pd@NCFs. The pore size distribution in Pd@NCFs is mainly within the range of 0.6–10 nm (inset of Fig. S2C). The average pore size is  $\sim 2.6$  nm, as calculated with the nonlocal density functional theory (NLDFT). The large surface area of  $335\text{ m}^2\text{ g}^{-1}$  for Pd@NCFs is attributed to the porous structure of Pd@NCFs samples.

XPS spectrum was carried out to examine the chemical compositions and elemental valences of Pd@NCFs. The XPS full spectrum of 3D Pd@NCFs further indicated that Pd@NCFs are composed of C, O, Pd, and N element. The contents of these elements are 78.7%, 1.8%, 4.8%, and 14.7%, respectively. Figure S2E demonstrates XPS spectra of N 1s region, the four main peaks at 402.7 eV, 400.8 eV, 398.9 eV, and 398.0 eV are fitted to oxidized N, graphitic N, pyrrolic N, and pyridinic N, respectively. In previous studies, the



wettability of carbon material in electrolyte can be improved by pyridinic N and both pyrrolic N, and the electronic conductivity can be enhanced by the graphitic N in carbon matrix [22]. The high nitrogen content combined with the large specific surface areas increases the electrochemically active areas, thus accelerating the transfer of electrons in electrochemical reactions. The high-resolution XPS spectrum of Pd 3d was deconvoluted into four peaks (Fig. S2F). The peaks of 340.6 eV and 335.4 eV are associated with spin-orbit states of Pd<sup>0</sup> [23]. The additional two weak peaks located at 342.1 eV and 357.1 eV are attributed to higher oxidation state (Pd<sup>II</sup>O). The results revealed the coexistence of Pd<sup>II</sup> and Pd<sup>0</sup> in Pd@NCFs, which are ascribed to the oxidation of metallic Pd.

### Electrochemical characterizations

The electrochemical properties of the electrodes were investigated by CV and EIS in 5 mM Fe(CN)<sub>6</sub><sup>4-/3-</sup> (Fig. 2). All the cyclic voltammograms (CVs) exhibit one reversible redox peaks (Fig. 2a). Compared with the low response with GCE, significantly increased peak current at Pd@NCFs/CGE was attributed to the high conductivity of Pd NPs and NCF. Furthermore, a significantly reduced peak potential difference ( $\Delta E_p$ ) from 115 mV (bare GCE) to 87 mV (Pd@NCFs/CGE) was acquired. Since a smaller  $\Delta E_p$  value indicates a faster electron transfer rate, porous carbon framework decorated with Pd NPs not only improves the conductivity but also increases their specific surface area. In addition, EIS was used to evaluate the conductive properties. The Nyquist diagram of EIS includes a low frequency linear portion corresponding to the diffusion and a higher frequency semicircular portion corresponding to the electrons transfer limited process [24]. Besides, the electron transfer resistance ( $R_{et}$ ) is equivalent to the diameter of the semicircle. The larger semicircle on the bare GCE (curve a) corresponds to a relatively large  $R_{et}$  value

of 250  $\Omega$  (Fig. 2b), while a smaller  $R_{et}$  value (90  $\Omega$ ) was obtained on Pd@NCFs/CGE (curve b), indicating an excellent charge transfer ability. These results revealed that uniformly distributed Pd NPs and graphene foam-like NCF are highly beneficial for improving the conductivity. Besides, as shown in Fig. S3, the electrochemical active surface area study was detailed in ESM.

### Electrochemical behaviors of UA and DA with modified electrodes

The electrocatalytic behaviors towards UA and DA with the Pd@NCFs/GCE electrode were investigated using DPV in 0.1 M KCl solutions that contained pH 7.0 PB, with and without the addition of DA. As shown in Fig. S4A and S4B, all the DPVs exhibits well-defined voltammetric peaks with 3D Pd@NCFs/GCE. Besides, two distinct signals at 0.36 V for UA and 0.18 V for DA were observed, respectively. As shown in Fig. S4A, the peak currents of both DA and UA increased with its increasing concentration without the presence of AA. As shown in Fig. S4B, after the addition of 10  $\mu$ M AA, the peak currents of both DA and UA did not change compared with that without the addition of AA (curve a and b). However, no response peak is seen for the AA sample in the presence of 10  $\mu$ M AA (curve b). As the DA and AA concentrations were fixed at 18  $\mu$ M and 25  $\mu$ M, respectively, the response for UA increased with increasing concentration of UA from 40 to 90  $\mu$ M. However, the peak currents of both DA and UA remained unaltered (curve e and f). Similar results were observed by fixing the concentration of AA and UA, and increasing the concentration of DA (curve f and g). Furthermore, there is no electrochemical response signal of AA, regardless of the presence or absence of AA (curve a-g). According to the literature, the concentration of AA in body fluids is much higher than that of DA [10]. With the present method, UA

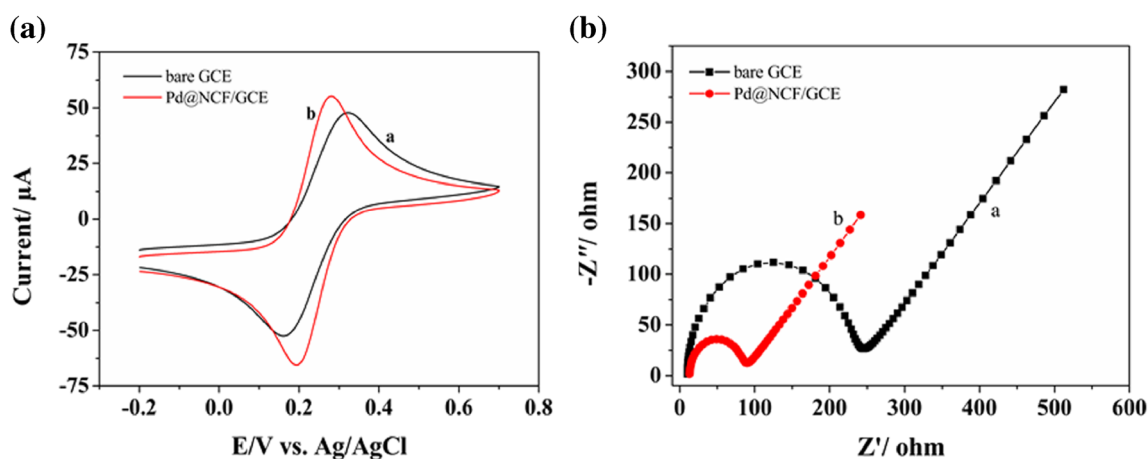


**Fig. 2** **a** CV and **b** EIS characterizations of bare GCE (curve a) and Pd@NCFs/GCE (curve b) in 0.1 M KCl solution containing 5 mM Fe(CN)<sub>6</sub><sup>4-/3-</sup>, respectively. Scan rate: 100 mV·s<sup>-1</sup>

and DA can be simultaneously analyzed by Pd@NCFs/GCE even as they coexist with a large amount of AA.

### Optimization of electrochemical parameters

The following parameters were optimized: (a) Sample pH value; (b) concentration of catalysts. Respective text and Figures on optimizations are given in the Electronic Supporting Material. In short, the following experimental conditions were found to give the best results: (a) Best sample pH value: 7; (b) 0.5  $\mu\text{L}$  of a 4  $\text{mg}\cdot\text{mL}^{-1}$  solution”.

### Individual and simultaneous detection of UA and DA in the presence of AA

#### Individual detection

The capability of Pd@NCFs/GCE for individual detection for DA or UA was examined in the absence of AA. DPVs and calibration plots of Pd@NCFs/GCE with various concentration of UA or DA are shown in Fig. 3. The oxidation peak currents of both UA and DA are proportional to their

concentrations (Fig. 3a, c). The linear fitting yielded the following relationship for DA:  $I_{DA} (\mu\text{A}) = (0.028 \pm 0.0001) C (\mu\text{M}) + (0.1455 \pm 0.001)$  ( $R^2 = 0.9901$ ) for the range of 0.5–50  $\mu\text{M}$  (Fig. 3b). Similarly, as shown the Fig. 3b, the linear fitting yielded the following relationship for UA:  $I_{UA} (\mu\text{A}) = (0.004 + 0.0001) C (\mu\text{M}) + (0.028 \pm 0.004)$  ( $R^2 = 0.999$ ) in the concentration range of 5–250  $\mu\text{M}$ . The detection limits (LOD) are calculated to be 0.132 and 0.295  $\mu\text{M}$  for DA and UA, respectively, based on  $S/N = 3$ .

The catalytic performance of Pd@NCFs/GCE for selective analysis of UA and DA was evaluated by DPV in pH 7.0 PB mixed with 25  $\mu\text{M}$  AA. As shown in Fig. 4a, UA concentration remained constant (50  $\mu\text{M}$ ) as DA concentration increased from 0.5 to 40  $\mu\text{M}$  with 25  $\mu\text{M}$  AA. Accordingly, response currents of DA are linearly increased with concentrations, and current signal of UA essentially remained constant, while AA did not yield any response signal (Fig. 4b). The regression equation is  $I_{DA} (\mu\text{A}) = (0.041 \pm 0.0002) C (\mu\text{M}) + (0.043 \pm 0.005)$  ( $R^2 = 0.9934$ ). Similar results for UA were acquired in the mixture of 5  $\mu\text{M}$  DA and 25  $\mu\text{M}$  AA (Fig. 4c), and the regression equation is  $I_{UA} (\mu\text{A}) = (0.003 \pm 0.0001) C (\mu\text{M}) + (0.004 \pm 0.0004)$  ( $R^2 = 0.9920$ ) with the

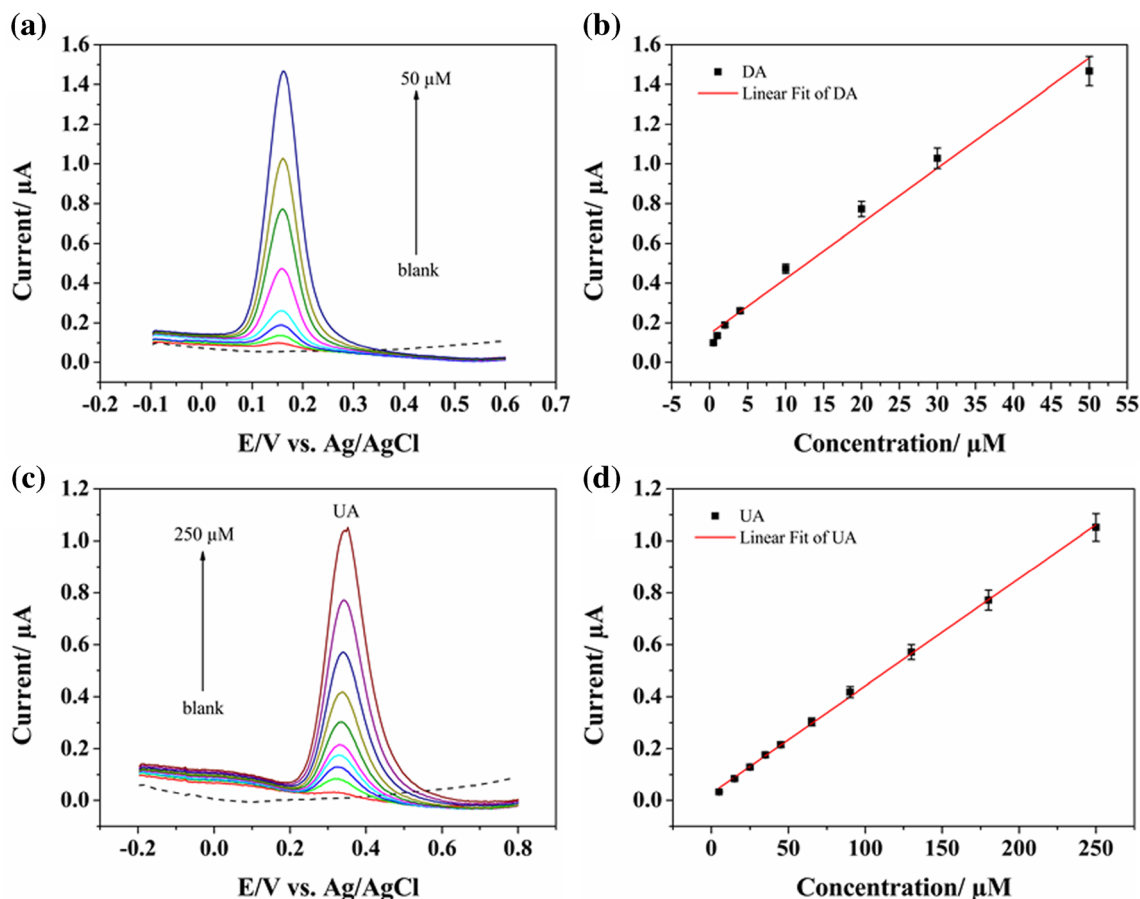


**Fig. 3** **a** DPVs of Pd@NCFs/GCE with increasing concentrations of DA; **b** Calibration plots of the corresponding oxidation peak currents vs the concentration for DA; **c** DPVs of Pd@NCFs/GCE with increasing

concentrations of UA; **d** Calibration plots of the corresponding oxidation peak currents vs the concentration for UA. Scan rate: 100  $\text{mV}\cdot\text{s}^{-1}$

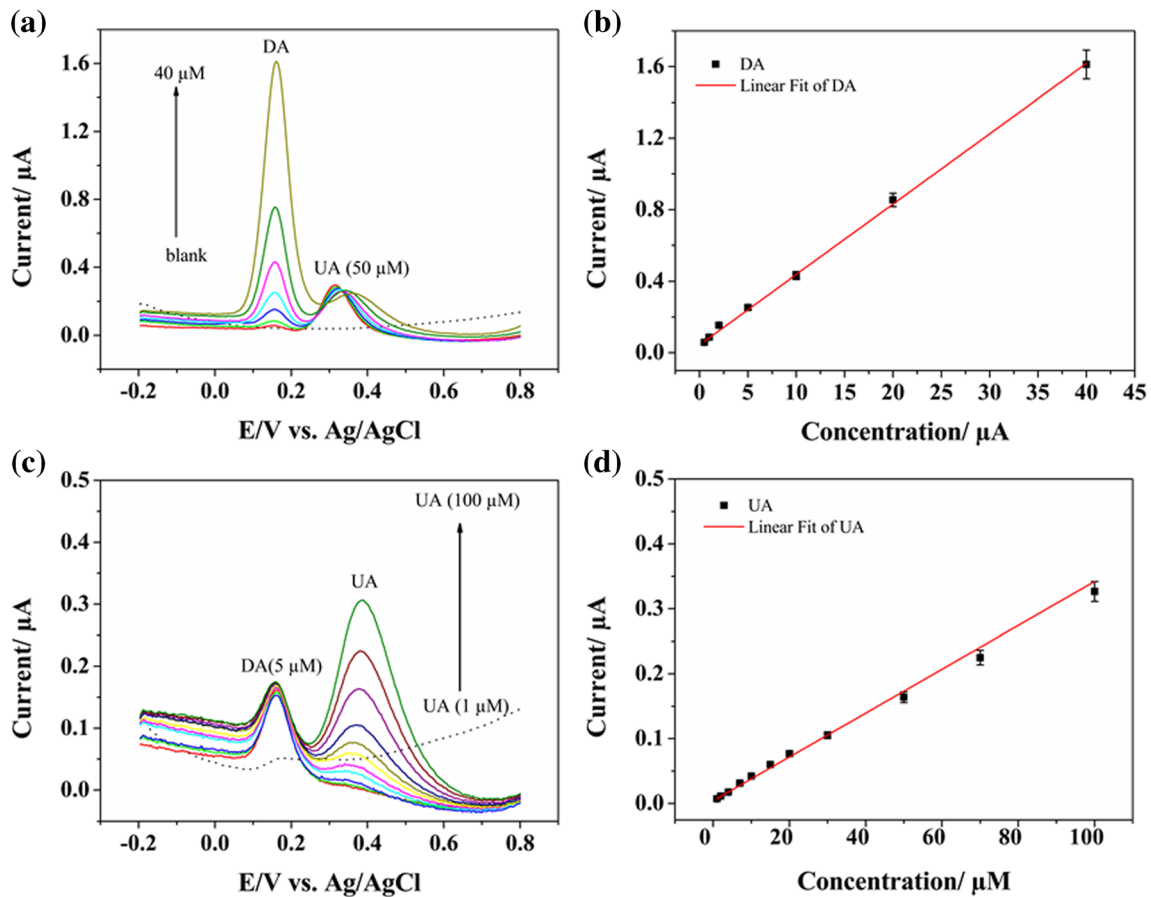


**Fig. 4** a DPVs of Pd@NCFs/GCE in pH 7.0 PB containing 50  $\mu\text{M}$  UA and various concentration of DA (from 0.5 to 40  $\mu\text{M}$ ); b The linear fit curve of the anodic peak current vs the concentration of DA; c DPVs of

Pd@NCFs/GCE in pH 7.0 PB containing 5  $\mu\text{M}$  DA and different concentration of UA (from 1 to 100  $\mu\text{M}$ ); d The linear fit curve of the anodic peak current vs the concentration of UA

linear range of 1 - 100  $\mu\text{M}$  (Fig. 4d). Besides, the calculated LODs ( $S/N = 3$ ) are 0.163  $\mu\text{M}$  and 0.873  $\mu\text{M}$  for DA and UA, respectively. These results indicate that there is no mutual interference between UA and DA.

### Simultaneous detection

Simultaneous analysis of UA and DA that are coexisting with AA by Pd@NCFs/GCE was also performed with DPV. As

shown in Fig. 5a, the responses currents of UA and DA increased simultaneously with increasing concentrations in the presence of 25  $\mu\text{M}$  AA. Figure 5b exhibits the linear response between currents and concentration from 0.5 to 100  $\mu\text{M}$  for DA, and the regression equation is  $I_{DA} (\mu\text{A}) = (0.017 \pm 0.0001) C (\mu\text{M}) + (0.140 \pm 0.002)$  ( $R^2 = 0.9926$ ) with an LOD of 0.076  $\mu\text{M}$  for DA. Figure 5c shows the regression equation is  $I_{UA} (\mu\text{A}) = (0.004 \pm 0.0001) C (\mu\text{M}) + (0.043 \pm 0.0001)$  ( $R^2 = 0.9933$ ) over the range of 0.5-230  $\mu\text{M}$  with an

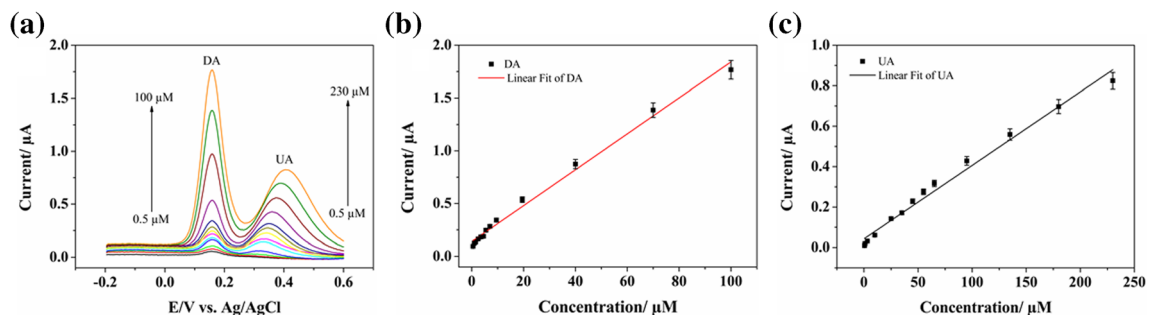


**Fig. 5** a DPV plots of the Pd@NCFs/GCE for simultaneous determination of DA and UA in pH 7.0 PB containing 25  $\mu\text{M}$  AA. b Calibration plots for DA c Calibration plots for UA

**Table 1** Comparison of the analytical performance of different modified electrodes for the determination of DA and UA

Electrode	Method	Analyte	Linear range ( $\mu\text{M}$ )	Detection limit ( $\mu\text{M}$ )	References
AgNC@PDA-NS/CGF/GCE	DPV	DA	2.5-130	0.25	[10]
		UA	10-130	1.9	
Nf/p(FeAni)-CNTsPE	DPV	DA	1-150	0.21	[11]
		UA	5-250	0.58	
Pt/RGO/GCE	DPV	DA	10-170	0.25	[25]
		UA	10-130	0.45	
MoS <sub>2</sub> /PEDOT/GCE	DPV	DA	1.0-80	0.52	[26]
		UA	2.0-50	0.95	
ANF-C700	DPV	DA	1.0-80	0.47	[27]
		UA	1.0-60	0.28	
HNP-AuAg/GCE	DPV	DA	5.0-335	0.2	[28]
		UA	5.0-425	1.0	
Pd@NCFs/GCE	DPV	DA	0.5-100	0.076	This work
		UA	0.5-230	0.107	

LOD of 0.107  $\mu\text{M}$ . In addition, the sensitivity for DA and UA is 153.2  $\text{nA}\cdot\mu\text{M}^{-1}\cdot\text{cm}^{-2}$  and 36.03  $\text{nA}\cdot\mu\text{M}^{-1}\cdot\text{cm}^{-2}$ , respectively. As shown in Table 1, the linear range and the LODs of the present method for DA and UA are superior or comparable to previously reported by other electrochemical sensors.

### Interference, reproducibility and stability

The potential interference of certain coexisting inorganic ions for analysis of UA and DA with Pd@NCFs/GCE were studied by DPV. Amperometric (*i-t*) measurement was used to investigate several potential interferents, including citric acid, glycine, glucose, KCl, Na<sub>2</sub>SO<sub>4</sub>, Na<sub>2</sub>CO<sub>3</sub>, NaNO<sub>3</sub>, epinephrine, adrenaline, serotonin, tyramine, tryptamine, and phenethylamine with the applied voltages of +0.36 V for UA and +0.18 V for DA, respectively (Fig. S8). Insignificant interferences (signal change <5%) showed that the aforementioned species (100-fold) have almost no interference for the analysis of UA and DA, indicating that this sensing system has good selectivity for UA and DA.

The reproducibility and stability of Pd@NCFs/GCE were tested by DPV. The reproducibility of Pd@NCFs/GCE was performed in PB (pH 7.0) mixed with 20  $\mu\text{M}$  DA, 80  $\mu\text{M}$  UA and 25  $\mu\text{M}$  AA by eight successive measurements (Fig. S9).

The calculated relative standard deviations (RSDs) are 2.4% for UA and 2.1% for DA, respectively. Besides, the stability of this sensing system was tested by storage in pH 7.0 PB at 4 °C for 35 days. The peak currents of UA and DA change by 2.0% and 3.4% with respect to their initial values, respectively, indicating that Pd@NCFs/GCE has good stability. These results demonstrate that Pd@NCFs/GCE exhibits high reproducibility, selectivity and stability.

### Real serum sample analysis

The Pd@NCFs/GCE sensing system was utilized to measure of DA and UA in deionized water and human serum sample with standard addition method. The standard addition method was usually used direct determination of small biomolecule in deionized water samples and comparison with HPLC, which is a proof for precision. To ensure the reliability in a low concentration range, the human serum sample was appropriately diluted with pH of 7.0 PSB. Figure S10 shows DPV responses of Pd@NCFs/GCE for serum sample after addition of various concentration of DA and UA. The concentration of UA in the original serum sample was found to be 42.8  $\mu\text{M}$ , and DA is not detected in the original serum sample under this experimental conditions. Satisfactory recoveries between

**Table 2** Determination of DA and UA in human serum from the present method ( $n=3$ )

Samples	Added ( $\mu\text{M}$ )	Found by proposed method ( $\mu\text{M}$ )		Found by HPLC ( $\mu\text{M}$ )		Recovery (%)		RSD (%)	
		DA	UA	DA	UA	DA	UA	DA	UA
Deionized water	5.0	4.88	4.95	5.23	5.38	97.6	99.0	0.25	0.30
	10.0	10.8	11.3	11.4	10.5	108.0	113.0	0.42	0.57
	15.0	16.3	15.7	15.4	14.3	108.7	104.7	0.64	1.56
Human serum	–	Not Found	32.5	Not Found	35.7	–	–	–	–



97.6% and 113.0% were obtained (Table 2). These results showed that this method has sufficient accuracy and precision and is suitable for analysis of UA and DA in practical sample.

## Conclusion

An electrochemical sensor based on 3D Pd@NCFs modified GCE was fabricated. The Pd@NCFs/GCE electro-catalyzes oxidation towards UA and DA, and simultaneously detect DA and UA in the presence of AA with high sensitivity, stability, good linearity and reproducibility. The Pd@NCFs/GCE was suitable for analysis of DA and UA in human serum sample, but in fact, it may not be suitable for samples containing complex matter and pH unstable system. Although still to be improved, the concept proposed in this paper provides a promising platform for simultaneously rapid and sensitive detection of small biomolecules in clinical applications with broad application prospects.

**Acknowledgments** This work was funded by the Sichuan Agricultural University Research Interest Project (Project No. 2018324).

## Compliance with ethical standards

**Conflict of interest** The authors declare that they have no competing interests.

**Ethical statement** This article does not contain any studies with human participants or animals performed by any of the authors. In this experiment, human serum samples were received from the Sichuan Agricultural University Hospital in China.

## References

- Rock KL, Kataoka H, Lai J-J (2012) Uric acid as a danger signal in gout and its comorbidities. *Nat Rev Rheumatol* 9:13
- Hirsch E, Graybiel AM, Agid YA (1988) Melanized dopaminergic neurons are differentially susceptible to degeneration in Parkinson's disease. *Nature* 334(6180):345–348
- Wightman RM, May LJ, Michael AC (1988) Detection of dopamine dynamics in the brain. *Anal Chem* 60(13):769A–793A
- Moghadam MR, Dadfarnia S, Shabani AMH, Shahbazikhah P (2011) Chemometric-assisted kinetic–spectrophotometric method for simultaneous determination of ascorbic acid, uric acid, and dopamine. *Anal Biochem* 410(2):289–295
- Chandra S, Singh VK, Yadav PK, Bano D, Kumar V, Pandey VK, Talat M, Hasan SH (2019) Mustard seeds derived fluorescent carbon quantum dots and their peroxidase-like activity for colorimetric detection of H<sub>2</sub>O<sub>2</sub> and ascorbic acid in a real sample. *Anal Chim Acta* 1054:145–156
- Kumbhat S, Shankaran DR, Kim SJ, Gobi KV, Joshi V, Miura N (2007) Surface plasmon resonance biosensor for dopamine using D3 dopamine receptor as a biorecognition molecule. *Biosens Bioelectron* 23(3):421–427
- Huang C, Chen X, Lu Y, Yang H, Yang W (2015) Electrogenerated chemiluminescence behavior of peptide nanovesicle and its application in sensing dopamine. *Biosens Bioelectron* 63:478–482
- Feng X, Zhang Y, Yan Z, Chen N, Ma Y, Liu X, Yang X, Hou W (2013) Self-degradable template synthesis of polyaniline nanotubes and their high performance in the detection of dopamine. *J Mater Chem A* 1(34):9775–9780
- Yang J, Strickler JR, Gunasekaran S (2012) Indium tin oxide-coated glass modified with reduced graphene oxide sheets and gold nanoparticles as disposable working electrodes for dopamine sensing in meat samples. *Nanoscale* 4(15):4594–4602
- Li Y, Jiang Y, Song Y, Li Y, Li S (2018) Simultaneous determination of dopamine and uric acid in the presence of ascorbic acid using a gold electrode modified with carboxylated graphene and silver nanocube functionalized polydopamine nanospheres. *Microchim Acta* 185(8):382
- Sroysee W, Chairam S, Amatatongchai M, Jarujamrus P, Tamuang S, Pimmongkol S, Chaicharoenwimolkul L, Somsook E (2018) Poly(m-ferrocenylaniline) modified carbon nanotubes-paste electrode encapsulated in nafion film for selective and sensitive determination of dopamine and uric acid in the presence of ascorbic acid. *J Saudi Chem Soc* 22(2):173–182
- Bellido-Milla D, Cubillana-Aguilera LM, El Kaoutit M, Hernández-Artiga MP, Hidalgo-Hidalgo de Cisneros JL, Naranjo-Rodríguez I, Palacios-Santander JM (2013) Recent advances in graphite powder-based electrodes. *Anal Bioanal Chem* 405(11):3525–3539
- Zhu C, Du D, Eychmüller A, Lin Y (2015) Engineering ordered and nonordered porous noble metal nanostructures: synthesis, assembly, and their applications in electrochemistry. *Chem Rev* 115(16):8896–8943
- Huang X, Li Y, Chen Y, Zhou E, Xu Y, Zhou H, Duan X, Huang Y (2013) Palladium-based nanostructures with highly porous features and perpendicular pore channels as enhanced organic catalysts. *Angew Chem Int Ed* 52(9):2520–2524
- Monai M, Montini T, Melchionna M, Duchoň T, Kúš P, Tsud N, Prince KC, Matolin V, Gorte RJ, Fornasiero P (2016) Phosphorus poisoning during wet oxidation of methane over Pd@CeO<sub>2</sub>/graphite model catalysts. *Appl Catal B* 197:271–279
- Zhang Y, Li M, Chen Q, Cai D, Zhan H (2017) Dendritic unzipped carbon nanofibers enable uniform loading of surfactant-free Pd nanoparticles for the electroanalysis of small biomolecules. *J Mater Chem B* 5(12):2254–2262
- Lu Z, Dai W, Lin X, Liu B, Zhang J, Ye J, Ye J (2018) Facile one-step fabrication of a novel 3D honeycomb-like bismuth nanoparticles decorated N-doped carbon nanosheet frameworks: ultrasensitive electrochemical sensing of heavy metal ions. *Electrochim Acta* 266:94–102
- Dong Y, Yu M, Wang Z, Liu Y, Wang X, Zhao Z, Qiu J (2016) A top-down strategy toward 3D carbon nanosheet frameworks decorated with hollow nanostructures for superior lithium storage. *Adv Funct Mater* 26(42):7590–7598
- Wang X, Zhang Y, Zhi C, Wang X, Tang D, Xu Y, Weng Q, Jiang X, Mitome M, Golberg D, Bando Y (2013) Three-dimensional strutted graphene grown by substrate-free sugar blowing for high-power-density supercapacitors. *Nat Commun* 4:2905
- Wang F, Wang K, Dong X, Mei X, Zhai Z, Zheng B, Lv J, Duan W, Wang W (2017) Formation of hierarchical porous graphene films with defects using a nanosecond laser on polyimide sheet. *Appl Surf Sci* 419:893–900
- Reina A, Jia X, Ho J, Nezhich D, Son H, Bulovic V, Dresselhaus MS, Kong J (2009) Large area, few-layer graphene films on arbitrary substrates by chemical vapor deposition. *Nano Lett* 9(1):30–35
- Deng W, Yuan X, Tan Y, Ma M, Xie Q (2016) Three-dimensional graphene-like carbon frameworks as a new electrode material for

- electrochemical determination of small biomolecules. *Biosens Bioelectron* 85:618–624
23. H-q S, Zhu Q, Zheng X-j, X-g C (2015) One-step synthesis of three-dimensional graphene/multiwalled carbon nanotubes/Pd composite hydrogels: an efficient recyclable catalyst for Suzuki coupling reactions. *J Mater Chem A* 3(19):10368–10377
  24. Lu Z, Zhang J, Dai W, Lin X, Ye J, Ye J (2017) A screen-printed carbon electrode modified with a bismuth film and gold nanoparticles for simultaneous stripping voltammetric determination of Zn(II), Pb(II) and Cu(II). *Microchim Acta* 184(12):4731–4740
  25. Xu T-Q, Zhang Q-L, Zheng J-N, Lv Z-Y, Wei J, Wang A-J, Feng J-J (2014) Simultaneous determination of dopamine and uric acid in the presence of ascorbic acid using Pt nanoparticles supported on reduced graphene oxide. *Electrochim Acta* 115:109–115
  26. Li Y, Lin H, Peng H, Qi R, Luo C (2016) A glassy carbon electrode modified with MoS<sub>2</sub> nanosheets and poly(3,4-ethylenedioxythiophene) for simultaneous electrochemical detection of ascorbic acid, dopamine and uric acid. *Microchim Acta* 183(9):2517–2523
  27. Taleb M, Ivanov R, Bereznev S, Kazemi SH, Hussainova I (2017) Ultra-sensitive voltammetric simultaneous determination of dopamine, uric acid and ascorbic acid based on a graphene-coated alumina electrode. *Microchim Acta* 184(12):4603–4610
  28. Hou J, Xu C, Zhao D, Zhou J (2016) Facile fabrication of hierarchical nanoporous AuAg alloy and its highly sensitive detection towards dopamine and uric acid. *Sensors Actuators B Chem* 225: 241–248

**Publisher's note** Springer Nature remains neutral with regard to jurisdictional claims in published maps and institutional affiliations.